International Journal of Thermal Sciences 51 (2012) 31–41

Contents lists available at SciVerse ScienceDirect

International Journal of Thermal Sciences

journal homepage: www.elsevier.com/locate/ijts

Transport phenomena in proton exchange membrane fuel cells and over-potential distribution of membrane electrode assembly

Dong-Myung Suh*, Seungbae Park

Department of Mechanical Engineering, State University of New York at Binghamton, Binghamton, NY 13902-6000, USA

ARTICLE INFO

Article history:
Received 26 April 2011
Received in revised form
16 August 2011
Accepted 22 August 2011
Available online 15 September 2011

Keywords:
Over-potential
PEMFC
MEA
Transport phenomena
Numerical model
Interface boundary model
Potential distribution

ABSTRACT

To study the coupled phenomena occurring in proton exchange membrane fuel cells, a two-phase, one-dimensional, non-isothermal model is developed. The model includes water phase change, proton transport in the membrane and electro-osmotic effect. The thinnest, but most complex layer in the membrane electrode assembly, catalyst layer, is considered an interfacial boundary between the gas diffusion layer and the membrane. Mass and heat transfer and electro-chemical reaction through the catalyst layer are formulated into equations, which are applied to boundary conditions for the gas diffusion layer and the membrane. Detail accounts of the boundary equations and the numerical solving procedure used in this work are given. The polarization curve is calculated at different oxygen pressures and compared with the experimental results. When the operating condition is changed along the polarization curve, the change of physicochemical variables in the membrane electrode assembly is studied. In particular, the over-potential diagram presents the usage of the electro-chemical energy at each layer of the membrane electrode assembly. As the fuel cell reaction becomes more limited by mass transfer, it is found that higher over-potential is uselessly concentrated on the cathode catalyst layer. The over-potential for the anode reaction was usually ignored in other studies, but the ratio of the anode over-potential to the cathode over-potential increases at a higher current condition. Water content is distributed more unevenly in the membrane, as the cell current is increased. That causes the proton conductivity of membrane to decrease and the water content to increase in the cathode side, which hampers O_2 transfer. The effect of electro-osmotic property, one of important property of membrane, on cell performance is also studied.

© 2011 Elsevier Masson SAS. All rights reserved.

1. Introduction

Fuel Cells are considered one of the most promising energy conversion devices for the 21st century, a time of growing concern about oil supplies and environmental pollution [1,2]. Among several types of fuel cells currently being studied, Polymer Electrolyte Membrane Fuel Cell (PEMFC) has drawn the most attention for the next generation power sources for transportation and portable applications [3]. The durability of membrane electrode assembly (MEA) has been enhanced and the manufacturing cost of PEMFC has been reduced. But the commercialization of PEMFC has not yet been achieved [4–6]. Further technological breakthroughs based on improved understanding of fuel cell operation, are required. Mathematical modeling and simulating the coupled phenomena occurring in MEA play an important role for understanding the fuel cell physics and the commercialization of this technology.

One of the most complicated part in modeling PEMFC is the catalyst layer. The catalyst layer, about 10 μm, is the thinnest layer in the MEA, but important reactions for fuel cells, hydrogen oxidation and oxygen reduction, occur in this layer. Three kinds of models for the CL can be found in the literature: interfacial model [7,8,25], pseudo-homogenous model [9,10], and agglomerate model [11,12]. In the interfacial model, the CL is assumed to be so thin that it is considered as an interface between the membrane and the GDL and all physical or chemical properties are constant throughout it. The uniform property of CL is also assumed in the pseudo-homogenous model, but the CL has a separate computational domain. In the third model, the CL is assumed to be agglomerate of carbon supported Pt, ionomer, and void space for gas transfer. Even though the homogenous model and agglomerate model more rigorously calculate transport phenomena inside the CL, their computational load is much heavier than that of the first model. In the simulation based on these models, the computational domain is

* Corresponding author. Tel.: +1 607 777 3565; fax: +1 607 777 4620.
E-mail address: dsuh3@binghamton.edu (D.-M. Suh).

1290-0729/$ – see front matter © 2011 Elsevier Masson SAS. All rights reserved.
doi:10.1016/j.ijthermalsci.2011.08.013

limited to the cathode side, and only selected effects are considered [10,12]. The interfacial model is the simplest one, but it is usually concerned with only the cathode side [7,8,25]. The over-potential for cathode reaction is just given as an input parameter or is calculated in a simple way. The over-potential for the anode reaction, and the potential distribution in the membrane are not calculated in all these models.

In the present model, the CL is regarded as an interface between the GDL and the membrane, but the whole range of MEA is concerned. The transport phenomena through the CL are formulated into the equations as presented in Section 2.3. The equations are applied to the boundary conditions for GDL and membrane. This approach can enhance computational stability and assure the balance of mass, charge and heat through MEA. This model can be effectively applied to a higher dimensional model which requires more computational consideration. The simulation results are compared with the experimental data. The distributions of gas concentration and potential through MEA are presented, when the cell condition is changed along polarization curves. In particular, the over-potential diagram shows how electro-chemical energy is consumed at each part of fuel cells and which step is a main hindrance to cell performance. It provides a good understanding of the cell performance with respect to over-potentials. The over-potential changes of anode and cathode are studied as the cell voltage is changed. The water distribution in membrane and its effect on the ionic conductivity are calculated. As one property of the membrane, the electro-osmotic effect on cell performance is also studied.

2. Numerical modeling

The MEA consists of five layers as shown in Fig. 1, viz., the cGDL (cathode Gas Diffusion Layer), the cCL (cathode Catalyst Layer), the membrane, the aCL (anode CL), and the aGDL (anode GDL). Oxygen and Hydrogen gases move through the GDL, and reach the CL. Electrons and water, which are the products of the reaction, also move through the GDLs. The water vapor can change into liquid during its movement when the temperature falls and the pressure increases. The liquid water can act as a barrier to the passage of reactant gases and consequently limit the electrical power of the fuel cell [13]. On the other hand, the membrane needs to be hydrated to maintain good conductivity for the protons. Therefore, the management of water becomes a critical factor in the design and operation of PEMC [14], and the behavior of water should be incorporated in the MEA modeling. In the aCL, hydrogen is oxidized into protons and electrons and in the cCL, oxygen is reduced to water. The proton and the electron transfer separately from the aCL to the cCL. The membrane through which the protons move, makes

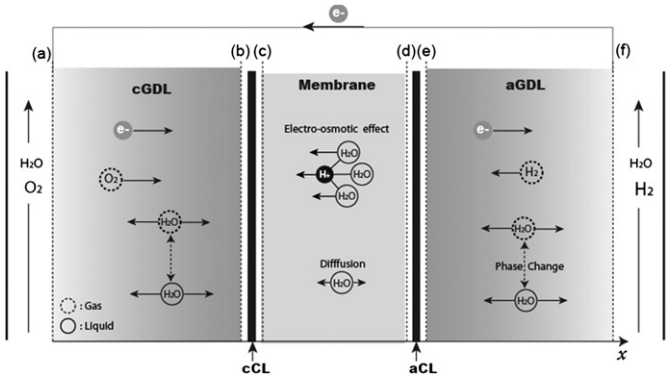

Fig. 1. Mass transfer through MEA in PEM fuel cells.

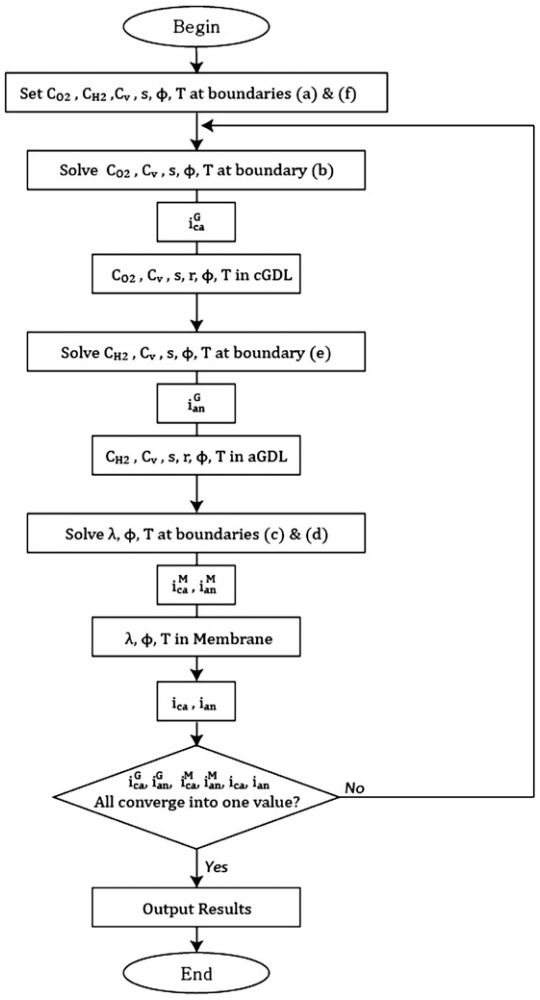

Fig. 2. Flow diagram of the solving procedure.

an integral connection between the oxidation and reduction, and completes the electro-chemical reaction in the PEMFC. Therefore, proton conductivity in the membrane heavily affects the reaction rate and the performance of a fuel cell. The conductivity depends on the amount of water absorbed in the membrane. All these correlated phenomena in the MEA are considered in the present model. The assumptions made in the model are as follows:

(i) The MEA is in a steady state and all variables are changed only in the thickness direction (1-dimensional).
(ii) The pressure gradient in the GDLs is negligible. Therefore, reactant gases are transferred by diffusion and liquid water is moved by the capillary effect.
(iii) Liquid or vapor water is absorbed by the membrane. But the absorbed water stays therein a liquid state. When water is desorbed from the membrane, it changes to vapor.
(iv) From the reaction at the cathode, liquid water is produced on the cGDL side.
(v) At any location within the MEA, liquid and gases are at the same temperature and heat is transferred by conduction.

The catalyst layer is modeled as an interfacial boundary between GDL and membrane. There are three computational domains, the two GDLs and the membrane, in the present model. The model is programmed into a simulation code in Mathematica (computational software).

2.1. Gas diffusion layer (GDL)

It is assumed that the pressure gradient is negligible in the GDL, and that gas species are transported by diffusion. To simplify it further, the diffusion is expressed with Fick's law rather than the Stefan–Maxwell equation because these two formulas lead practically to the same results when an appropriate diffusion coefficient is used [12,15]. So the transport of species is described as

$$\frac{\mathrm{d}}{\mathrm{d}x}\left(D_{\mathrm{i}}^{\mathrm{G}}\frac{\mathrm{d}}{\mathrm{d}x}C_{\mathrm{i}}\right) = 0 \tag{1}$$

where C_{i} is the mass concentration of species i, and $D_{\mathrm{i}}^{\mathrm{G}}$ is the effective diffusivity of species i in the GDL. The effective diffusivity is defined using the Bruggeman model [16] which correlates these factors with the diffusivity,

$$D_{\mathrm{i}}^{\mathrm{G}} = D_{\mathrm{i}}(1-s)^{1.5}\varepsilon^{1.5} \tag{2}$$

In Eqn. (2), D_{i} is the diffusivity of species i in the gas mixture, ε is the porosity of the GDL and s is the liquid water saturation. The diffusion equation for water vapor contains a source term which accounts for the phase change of water in GDL.

$$\frac{\mathrm{d}}{\mathrm{d}x}\left(-D_{\mathrm{v}}^{\mathrm{G}}\frac{\mathrm{d}C_{\mathrm{v}}}{\mathrm{d}x}\right) = -r \tag{3}$$

The subscript v denotes water vapor and r is the volumetric condensation rate of water which is given as Eqn. (4) [17].

$$r = \varepsilon(1-s)M_{\mathrm{v}}\gamma\frac{p_{\mathrm{sat}}-p_{\mathrm{v}}}{R_{\mathrm{g}}T} = \varepsilon(1-s)\gamma(C_{\mathrm{sat}}-C_{\mathrm{v}}) \tag{4}$$

where γ is the volumetric phase change coefficient. The water vapor saturation pressure (p_{sat}) is given by [18]

$$\log_{10}p_{\mathrm{sat}} = -2.1794 + 0.02953\mathbb{C} - 9.1837\times10^{-5}\mathbb{C}^2 + 1.4454\times10^{-7}\mathbb{C}^3 \tag{5}$$

where $\mathbb{C}$ is the temperature in Celsius degree.

The transport of liquid water is driven by capillary action, and its mass flux ($\dot{m}_{\mathrm{l}}$) is given as [19]

$$\dot{m}_{\mathrm{l}} = -\frac{\rho_{\mathrm{l}}KK_{\mathrm{rl}}}{\mu_{\mathrm{l}}}\nabla p_{\mathrm{c}} = -\left(\frac{\rho_{\mathrm{l}}K}{\mu_{\mathrm{l}}}\right)K_{\mathrm{rl}}\left(\frac{\mathrm{d}P_{\mathrm{c}}}{\mathrm{d}s}\right)\nabla s \tag{6}$$

where ρ_{l} and μ_{l} are the density and viscosity of liquid water, and P_{c} is the capillary pressure. K_{rl} is the relative permeability of the GDL, which is set to s^3 [17]. Then, the mass balance equation for liquid water is given as

$$\nabla\cdot\dot{m}_{\mathrm{l}} = -\frac{\mathrm{d}}{\mathrm{d}x}\left(\frac{\rho_{\mathrm{l}}K}{\mu_{\mathrm{l}}}s^3\left(\frac{\mathrm{d}P_{\mathrm{c}}}{\mathrm{d}s}\right)\frac{\mathrm{d}s}{\mathrm{d}x}\right) = r \tag{7}$$

The electrical charges are also conserved in the GDL and the charge balance equation is expressed in terms of electrical potential (ϕ) using Ohm's law,

$$\nabla\cdot i = \nabla\cdot\left(\sigma^{\mathrm{G}}\nabla\phi\right) = \sigma^{\mathrm{G}}\frac{\mathrm{d}^2\phi}{\mathrm{d}x^2} = 0 \tag{8}$$

where i is the charge flux, or current density and σ^{G} is the electrical conductivity of the GDL.

For heat transfer, the conduction rate is balanced by the heat generation from Joule heat and water condensation. Thus, the governing equation for heat transfer is written as

$$-\kappa^{\mathrm{G}}\frac{\mathrm{d}^2T}{\mathrm{d}x^2} = \nabla\cdot\left(\sigma^{\mathrm{G}}\nabla\phi\right) + r\Delta H = \sigma^{\mathrm{G}}\left(\frac{\mathrm{d}\phi}{\mathrm{d}x}\right)^2 + r\Delta H \tag{9}$$

where κ^{G} is the thermal conductivity of the GDL and ΔH is the condensation heat of water. Heat transfer induced by vapor phase diffusion, the so-called heat pipe effect [35], is not included in this model. If the effect is considered, the heat could transfer more quickly and the maximum temperature deviation in MEA, which is calculated 3 °C at C1 condition in Fig. 3(b) using the present model, would be smaller. So the temperature effect on the cell performance could be much less.

2.2. Membrane

Only the transport of protons and water molecules is considered in this layer, since the transport of the other species (H_2, O_2) is negligible [20]. Proton transfer in the membrane is formulated with the charge balance equation.

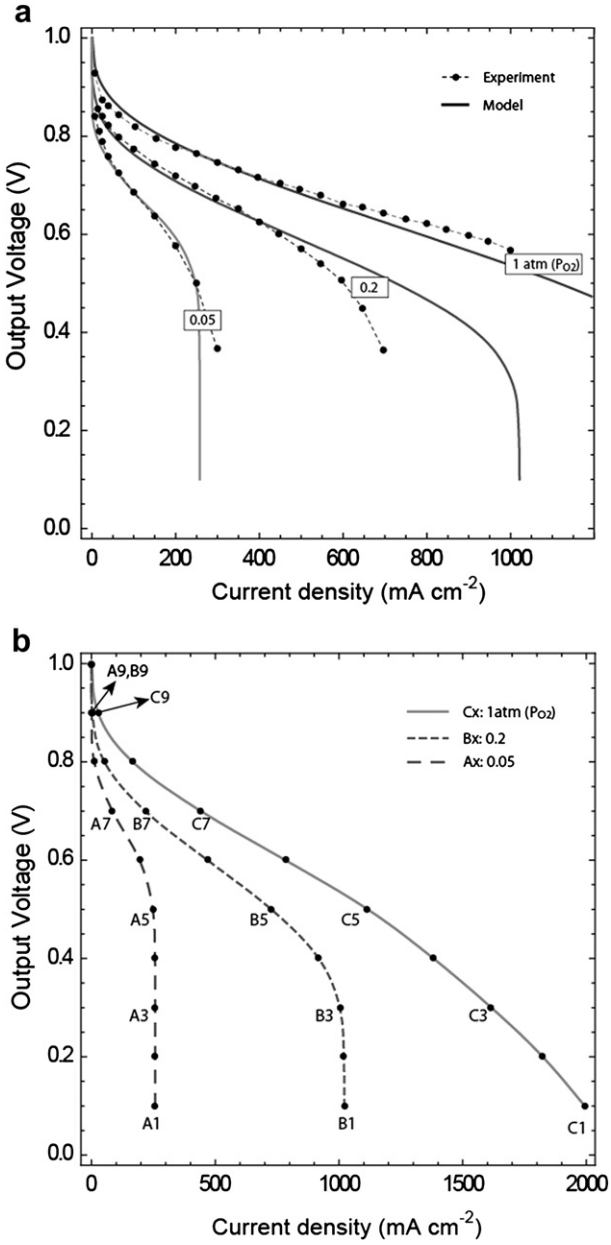

Fig. 3. (a). Comparison of polarization curve from the model with the experiments [28]. (b). Points where transport phenomena are studied.

$$\nabla\cdot i = \nabla\cdot\left(\sigma^{M}\nabla\phi\right) = \frac{d}{dx}\left(\sigma^{M}\frac{d\phi}{dx}\right) = 0, \tag{10}$$

where i is the charge flux of protons and ϕ is its potential, and σ^{M} is ionic conductivity which is a function of the water content in the membrane. In the present work, the empirical equation presented by Springer et al. [18] is used for the ionic conductivity in the membrane.

$$\sigma^{M} = (0.5139\lambda - 0.326)e^{1268\left(\frac{1}{303}-\frac{1}{T}\right)} \tag{11}$$

where λ is the membrane water content defined as the Eqn. (12) [20].

$$\lambda = \left(\frac{C_l}{M_l}\right)\Big/\left(\frac{\rho_M}{EW_M}\right) \tag{12}$$

where ρ_M and EW_M are the density and the equivalent molecular weight of the membrane, and C_l and M_l are the mass concentration and the molecular weight of liquid water.

Water transport in the membrane is modeled with two processes: one is diffusion caused by a concentration gradient, and the other is electro-osmotic drag. So, the mass balance equation of water is written as

$$\nabla\cdot\dot{m}_l = -\frac{d}{dx}\left(D_l^{M}\frac{dC_l}{dx}\right) - \frac{M_l}{F}\frac{d}{dx}\left(n_d\sigma^{M}\frac{d\phi}{dx}\right) = 0 \tag{13}$$

where D_l^{M}, the membrane water diffusivity, is given by the equation of Motupally et al. [21].

$$D_l^{M} = \begin{cases} 3.1\times10^{-7}\lambda\left(e^{0.28\lambda}-1\right)e^{-\frac{2346}{T}}, & \lambda < 3 \\ 4.17\times10^{-8}\lambda\left(161e^{-\lambda}+1\right)e^{-\frac{2346}{T}}, & \lambda \geq 3 \end{cases} \tag{14}$$

The coefficient of electro-osmotic drag (n_d) is given as the function of λ [22].

$$n_d = \begin{cases} 0.2\lambda, & \lambda < 5 \\ 1, & 5 < \lambda < 14 \\ 0.1875\lambda - 1.625, & \lambda > 14 \end{cases} \tag{15}$$

In the membrane, the heat conduction rate is balanced by the heat generated when protons move through the membrane. Thus, the heat transfer equation is written as

$$-\kappa^{M}\frac{d^2T}{dx^2} = \sigma^{M}\left(\frac{d\phi}{dx}\right)^2 \tag{16}$$

where κ^{M} is the thermal conductivity of the membrane.

2.3. Catalyst layer (CL)

The catalyst layer is the thinnest layer in the MEA, but it is the most complex and important part for the fuel cell operation. The CL is considered as an interfacial boundary between gas diffusion layer and membrane. Mass and heat transfer and electro-chemical reaction through the CL are formulated into equations, which provide the boundary conditions for the adjacent layers: GDL and membrane. The reaction at the cCL is different from the reaction at the aCL and the equations are developed separately at each CL.

2.3.1. Cathode catalyst layer (cCL)

The following reduction reaction occurs at the cCL.

$$\frac{1}{2}O_2(g) + 2H^{+} + 2e^{-} \Rightarrow H_2O(l) \tag{17}$$

The water produced from the reaction is assumed to be in a liquid state. The rate of the cathode reaction, Eqn. (17), is related to the electrical current generated from the reaction and the current is given by the Butler–Volmer equation [23].

$$i_{ca} = (1-s)i_{ca}^{ref}\left(\left(\frac{C_{O_2}}{C_{O_2}^{ref}}\right)^{\nu}\mathrm{Exp}\left[\frac{\beta_{ca}\cdot 2F}{R_gT}\left(\phi^{c}+E_{ca}^{ref}-\phi^{b}\right)\right] - \mathrm{Exp}\left[\frac{-(1-\beta_{ca})\cdot 2F}{R_gT}\left(\phi^{c}+E_{ca}^{ref}-\phi^{b}\right)\right]\right) \tag{18}$$

In Eqn. (18), s is the liquid water saturation at position (b). The cathode reaction is decreased to the extent that the oxygen transfer is blocked by liquid water [16,24]. i_{ca}^{ref} and $C_{O_2}^{ref}$ are the cathode exchange current density and the mass concentration of oxygen at the reference state, respectively. At the reference state, the partial pressure of oxygen is 1 atm and the temperature is 60 °C. The i_{ca}^{ref} is determined by the characteristics of CL (thickness, morphology and the amount of Pt loading, etc.), so that it becomes a specific parameter to each MEA. In the present work, the value is chosen by fitting the model to the experimental data. The concentration exponent of oxygen, ν, is also determined by fitting. The constant, β_{ca}, is the cathode symmetry factor. The variables, ϕ^{b} and ϕ^{c}, are the potentials at positions (b) and (c) shown in Fig. 1. E_{ca}^{ref} is the electro-chemical potential at the reference state and is given as a function of temperature [16].

$$E_{ca}^{ref} = 1.23 - 0.9\times10^{-3}(T-298) \tag{19}$$

The term $(\phi^{c}+E_{ca}^{ref}-\phi^{b})$ defines the over-potential (η_{ca}) at the cathode. At a steady state, the rate of the electro-chemical reaction is the same as the rate of oxygen consumption, which is the oxygen mass flux into the catalyst layer. Therefore, we obtain the following equation at the boundary (b),

$$i_{ca} = -\left(D_{O_2}^{G}\frac{dC_{O_2}}{dx}\Big|_{b}\right)\frac{4F}{M_{O_2}} \tag{20}$$

Using Eqn. (18), Eqn. (20) becomes an equation with respect to the mass concentration of oxygen at position (b),$C_{O_2}^{b}$. The $C_{O_2}^{b}$ calculated from the equation is applied to the boundary value of the diffusion equation in the cGDL. The $C_{O_2}^{b}$ also gives the current density from Eqn. (20), which is denoted as i_{ca}^{G}. Then, ϕ^{b} is calculated by the following equation.

$$i_{ca}^{G} = \left(\sigma^{G}\frac{d\phi}{dx}\Big|_{b}\right) \tag{21}$$

The electrical potential at position (c) is calculated from the following equation.

$$i_{ca} = \left(\sigma^{M}\frac{d\phi}{dx}\Big|_{c}\right) \tag{22}$$

At this time, the above equation is solved for ϕ^{c} using the pre-calculated variables. Then one can determine the cathode current density toward the membrane. The density is denoted as i_{ca}^{M}.

Water can move through the catalyst layer, from or to the membrane in the assumed way in (iii). The mass flux of water at position (b) must be equal to the flux at position (c) under a steady state condition. In other words, the diffusive flux in the GDL is equal to the sum of the diffusive flux and electro-osmotic flux in the membrane,

$$-D_V^{G}\frac{dC_v}{dx}\Big|_{b} = -\left(D_l^{M}\frac{dC_l}{dx}\Big|_{c}\right) - \frac{M_l}{F}\left(n_d\ \sigma^{M}\frac{d\phi}{dx}\Big|_{c}\right) \tag{23}$$

The water concentration (C_l) in the membrane is related to the water content (λ) through Eqn. (12). Water in the membrane has an

equilibrium relationship with water in the GDL. According to Springer et al. [18], the λ in the membrane was increased up to 14 with the activity (a) of vapor water in its surroundings and the relationship was given as Eqn. (24).

$$\lambda_v = \begin{cases} 0.043 + 17.81a - 39.85a^2 + 36.0a^3, & 0 < a < 1 \\ 14, & a \geq 1, \end{cases} \quad (24)$$

where

$$a = \frac{P_v}{P_{sat}} = \frac{C_v}{C_{sat}} \quad (25)$$

When the membrane contacts liquid water, the water content in the membrane measured 22.

$$\lambda_l = 22 \quad (26)$$

In the present work, water can exist in both liquid and vapor states in GDL. So the membrane takes up water in the two states from GDL and the water content at position (c) can be calculated as the following equation.

$$\lambda = (1-s)\lambda_v + s\lambda_l \quad (27)$$

Eqn. (23) can be solved for C_v^b, using Eqn. (12) and Eqn. (24)–(27) and the λ at position (c) can be determined. The water saturation (s^b) at position (b) is calculated from the mass balance equation, Eqn. (28), where the liquid flux by capillary effect is equal to the liquid water generation from the cathode reaction.

$$\dot{m}_l^b = -\frac{d}{dx}\left(\frac{\rho_l K}{\mu_l} S^3 \left(\frac{dP_c}{ds}\right)\frac{ds}{dx}\right)\Big|_b = \frac{M_l}{2F} i_{ca}^G \quad (28)$$

The condition for heat transfer at the interface is complicated because of the existence of several heat fluxes. The heat transfer through this layer is treated as the transfer through a contact having a specific thermal conductance [25]. There is a heat flux from the cathode reaction, too. This flux can be divided into two parts: an irreversible one from the over-potential, and a reversible one from the entropy change [26]. Another flux arises from absorption/desorption of water on membrane. The heat from absorption is assumed to be equal to the condensation heat of water [27]. Thus, the total heat flux equation at the boundary (b) is given as

$$-\kappa^G \frac{dT}{dx}\Big|_b = -h_{ca}\left(T^c - T^b\right) - i_{ca}^G\left(\eta_{ca} - \prod_{ca}\right) + D_v^G \frac{dC_v}{dx}\Big|_b \cdot \Delta H \quad (29)$$

where h_{ca} is the thermal contact conductance and Π_{ca} is the Peltier coefficient representing the reversible potential of the cathode reaction [26]. T^b can be solved from Eqn. (29). At position (c), the contact heat transfer is equal to the heat conduction into the membrane. Hence T^c is solved from the following equation.

$$-\kappa^M \frac{dT}{dx}\Big|_c = -h_{ca}\left(T^c - T^b\right) \quad (30)$$

2.3.2. Anode catalyst layer (aCL)

At the aCL, hydrogen is oxidized into protons and electrons as follows.

$$H_2(g) \Rightarrow 2H^+ + 2e^- \quad (31)$$

The rate of the anode reaction can also be written in the Butler–Volmer form [17],

$$i_{an} = (1-s)\cdot i_{an}^{ref}\left(\left(\frac{C_{H_2}}{C_{H_2}^{ref}}\right)\mathrm{Exp}\left[\frac{\beta_{an}\cdot 2F}{R_g T}\left(\phi^e - \phi^d - E_{an}^{ref}\right)\right] - \mathrm{Exp}\left[\frac{-(1-\beta_{an})\cdot 2F}{R_g T}\left(\phi^e - \phi^d - E_{an}^{ref}\right)\right]\right) \quad (32)$$

The concentration $C_{H_2}^{ref}$ is calculated at the reference state in the same way that $C_{O_2}^{ref}$. i_{an}^{ref} is the anode exchange current density. The reference potential of the anode reaction, E_{an}^{ref}, is zero. The anode over-potential (η_{an}) is given as $(\phi^e - \phi^d)$. In a steady state condition, the rate of the above reaction is the same as the rate of hydrogen consumption which is determined by the mass flux of hydrogen to the catalyst layer.

$$i_{an} = -\left(D_{H_2}^G \frac{dC_{H_2}}{dx}\Big|_e\right)\frac{2F}{M_{H_2}} \quad (33)$$

The mass concentration ($C_{H_2}^e$) of hydrogen at position (e) is determined from solving Eqn. (33) and then i_{an}^G is evaluated with $C_{H_2}^e$. i_{an}^G, in turn, gives ϕ^e using the following equation.

$$i_{an}^G = \left(\sigma^G \frac{d\phi}{dx}\Big|_e\right) \quad (34)$$

The electrical potential (ϕ^d) at position (d) can be solved with Eqn. (35),

$$i_{an} = \left(\sigma^M \frac{d\phi}{dx}\Big|_d\right) \quad (35)$$

From ϕ^d and Eqn. (37), another current density (i_{an}^M) can be calculated.

The balance equation for the mass flux of water through the aCL is set up as the same form as Eqn. (23), the mass flux through the cCL.

$$-D_v^G \frac{dC_v}{dx}\Big|_e = -\left(D_l^M \frac{dC_l}{dx}\Big|_d\right) - \frac{M_l}{F}\left(n_d\ \sigma^M \frac{d\phi}{dx}\Big|_d\right) \quad (36)$$

The mass concentration (C_v^e) of water vapor at position (e) and the membrane water content (λ^d) are solved using the Eqn. (36) and Eqns. (24)–(26). Liquid water is not produced by the anode reaction (31), and water flux is zero at position (e).

$$\dot{m}_l^e = -\frac{d}{dx}\left(\frac{\rho_l K}{\mu_l} S^3 \left(\frac{dP_c}{ds}\right)\frac{ds}{dx}\right)\Big|_e = 0 \quad (37)$$

The heat flux at positions (d) and (e) can also be written in the same way as at positions (c) and (b). T^e and T^d can be calculated from Eqns. (38) and (39) respectively.

$$-\kappa^G \frac{dT}{dx}\Big|_e = -h_{an}\left(T^e - T^d\right) + i_{an}^G\left(\eta_{an} - \prod_{an}\right) + D_v^G \frac{dC_v}{dx}\Big|_e \cdot \Delta H \quad (38)$$

$$-\kappa^M \frac{dT}{dx}\Big|_d = -h_{an}\left(T^e - T^d\right) \quad (39)$$

where h_{an} is the thermal contact conductance at the anode interface.

3. Numerical solution

The differential equations governing the transport phenomena in MEA, are changed into finite difference form [22]. A computation software, *Mathematica*®, is used to solve the equations numerically. Fig. 2 shows the flow chart of the numerical solution procedure. First, the boundary values at (a) and (f) are provided as inputs to the

program. Note that the potential is set to zero at the anode side (f) and an output cell voltage is given at the cathode side (a). The boundary values are also used to initialize the internal variables inside the aGDL and cGDL. As for the initial values inside the membrane, water content, potential and temperature are set to 1, −0.0001 V, 60 °C, respectively. Then the variables in the three layers are updated repeatedly in the Gauss-Seidel Iteration loop. In each layer, the interfacial boundary value is calculated prior to the internal variables. In fact, the interfacial values are solved by the Newton–Raphson method. For example, the interfacial condition for oxygen at position (b), given by Eqn. (22) can be rewritten into the finite difference form.

$$\left(1-s^{\mathrm{b}}\right)i_{\mathrm{ca}}^{\mathrm{ref}}\left(\left(\frac{C_{\mathrm{O_2}}^{\mathrm{b}}}{C_{\mathrm{O_2}}^{\mathrm{ref}}}\right)^{\mathrm{v}}\mathrm{Exp}\left[\frac{\beta_{\mathrm{ca}}\cdot 2F}{R_{\mathrm{g}}T^{\mathrm{b}}}\left(\phi^{\mathrm{c}}+E_{\mathrm{ca}}^{\mathrm{ref}}-\phi^{\mathrm{b}}\right)\right]-\mathrm{Exp}\left[\frac{-(1-\beta_{\mathrm{ca}})\cdot 2F}{R_{\mathrm{g}}T^{\mathrm{b}}}\left(\phi^{\mathrm{c}}+E_{\mathrm{ca}}^{\mathrm{ref}}-\phi^{\mathrm{b}}\right)\right]\right)=-\frac{D_{\mathrm{O_2}}^{\mathrm{G,b}}}{\Delta x}\left(C_{\mathrm{O_2}}^{\mathrm{b}}-C_{\mathrm{O_2}}^{\mathrm{b-1}}\right)\frac{4F}{M_{\mathrm{O_2}}} \tag{40}$$

where Δx is the finite length of cGDL and the superscripts, b, b−1, and c, indicate the positions where the variables are evaluated. Now Eqn. (40) is solved numerically with respect to $C_{\mathrm{O_2}}^{\mathrm{b}}$, using the other variables previously calculated. Then the current density ($i_{\mathrm{ca}}^{\mathrm{G}}$) at position (b) is calculated from the right hand side of Eqn. (40) and the oxygen concentrations inside cGDL are calculated using the Gauss-Seidel iteration method.

The same calculations are processed on the other variables and then in the other layers. The current density ($i_{\mathrm{an}}^{\mathrm{G}}$) at (e) is based on the gradient of hydrogen concentration, Eqn. (33), but the current densities ($i_{\mathrm{ca}}^{\mathrm{M}}, i_{\mathrm{an}}^{\mathrm{M}}$) at (c) and (d) are based on the potential gradients, Eqns. (22) and (35). Convergence is tested with the above four current densities and another two current densities ($i_{\mathrm{ca}}, i_{\mathrm{an}}$) from Eqns. (18) and (32). These six values should be equal at the steady state condition. At every iteration of the big loop, all the variables are updated and the six current densities are recalculated. When the maximum deviation of the six data is smaller than 10^{-8} mA cm^{-2}, the current density is considered to converge into one value. Finally the iterative calculation stops and solutions are printed out.

4. Results and discussion

To validate the model developed here, it is compared with the published experimental data in Rho et al. [28], where the effect of oxygen pressure on the cell performance is studied. The simulation is performed under the conditions of three different O_2 pressures, with the parameters given in Table 1. The polarization curves from the simulation are presented in Fig. 3(a). The curves demonstrate the initial voltage drop for activating the catalyst, the steady decline of voltage with the increasing current, and then the limited current density at low output voltage. The important features of a polarization curve are well simulated and the result shows a close agreement with the experiment at each condition.

However, this model is one-dimensional one, and it cannot include the change of transport phenomena along the flow channel. In fact, a measured polarization curve reflects an average performance over the whole area of MEA. So, a multi-dimensional model could predict more precisely the fuel cell behavior and give a better correlation at 0.2 atm and higher current condition in Fig. 3(a). Now this model is being extended into a three-dimensional, CFD based fuel cell model.

Fig. 3(b) shows some labeled points on the calculated curves, at which transport phenomena are studied in the following sections.

Table 1
Model parameters.

	Parameter	Symbol	Value
Geometry	Thickness of Membrane (m)		250E-6
	Thickness of GDL (m)		100E-6
	Porosity of GDL	ε	0.5
Diffusivity	Oxygen (m^2 s^{-1})	$D_{\mathrm{O_2}}^{\mathrm{G}}$	3.03E-6
	Hydrogen (m^2 s^{-1})	$D_{\mathrm{H_2}}^{\mathrm{G}}$	11.4E-6
	Water Vapor (m^2 s^{-1})	$D_{\mathrm{v}}^{\mathrm{G}}$	3.45E-6
Liquid Water (l)	Condensation/Evaporation Rate (s^{-1}) [17]	γ	900
	Absolute Permeability (m^2) [17]	K	2.55E-13
	Viscosity (kg m^{-1}s^{-1}) [17]	μ_{l}	40.5E-5
	dP_{c}/ds (Pa) [17]	dP_{c}/ds	30,321
Membrane	Electrical Conductivity of GDL (S m^{-1}) [34]	σ^{D}	120
	Equivalent Molecular Weight (kg mol^{-1}) [20]	$\mathrm{EW_M}$	1.1
	Density (kg m^{-3}) [20]	ρ_{M}	1980.
Electro-chemical	Cathodic Exchange Current Density at Reference State (A m^{-2})	$i_{\mathrm{ca}}^{\mathrm{ref}}$	0.0132
	Anodic Exchange Current Density at Reference State (A m^{-2})	$i_{\mathrm{an}}^{\mathrm{ref}}$	1800
	Cathodic Symmetry Factor [30]	β_{ca}	0.5
	Anodic Symmetry Factor [30]	β_{an}	0.5
	Concentration Exponent of Oxygen	ν	1.5
Thermal	Conductivity of GDL (W m^{-1}K^{-1}) [26]	κ^{G}	1.5
	Conductivity of Membrane (W m^{-1}K^{-1}) [26]	κ^{M}	0.25
	Contact Conductance at Cathode Side (W m^{-2}K^{-1}) [35]	h_{ca}	0.3/10^{-5}
	Contact Conductance at Anode Side (W m^{-2}K^{-1}) [35]	h_{an}	0.3/10^{-5}
	Condensation Heat of Water (J kg^{-1}) [26]	ΔH	2.315 E6
	Peltier Coefficient of Cathode (V) [26]	Π_{ca}	−0.24T/298
	Peltier Coefficient of Anode (V) [26]	Π_{an}	−0.013T/298
Operating Condition	Operating Temperature (°C)	T_{i}	60
	Mass Concentration of O_2 at (a) (kg m^{-3})	$C_{\mathrm{O_2}}\vert$a	1.136 (1 atm)
	Mass Concentration of H_2O at (a) (kg m^{-3})	$C_{\mathrm{H_2O}}\vert$a	0.1965 (p_{sat})
	Liquid Water Saturation at (a)	$s\vert$a	0.1
	Mass Concentration of H_2 at (f) (kg m^{-3})	$C_{\mathrm{H_2}}\vert$f	0.0716 (1 atm)
	Mass Concentration of H_2O at (f) (kg m^{-3})	$C_{\mathrm{H_2O}}\vert$f	0.1965 (p_{sat})
	Liquid Water Saturation at (f)	$s\vert$f	0.0

The labels, A, B, and C represent the three different oxygen pressure and the following number indicates the output voltage (V_{out}).

4.1. Potential distribution

The potential distribution in the MEA at C1 condition is shown in Fig. 4. It has positive slopes in the GDLs and membrane, which indicates that the electrons move in the positive x direction in the GDLs, but the protons move in the opposite direction in the membrane [13]. The gradient of potential in the GDLs is constant and small, because the electron conductivity is constant and much higher than the ionic conductivity of the membrane. The ionic conductivity depends on the water content in the membrane, and the gradient of potential in the membrane is changed according to the local water content. The anode over-potential (η_{an}) is calculated as the potential drop at the interface (d|e), but the cathode over-potential (η_{ca}) is the difference between ϕ^{b} and $(\phi^{\mathrm{c}}+E_{\mathrm{ca}}^{\mathrm{ref}})$. The η_{ca} is higher than the η_{an} as in the figure, because the cathode reaction is much more sluggish that the anode reaction [29].

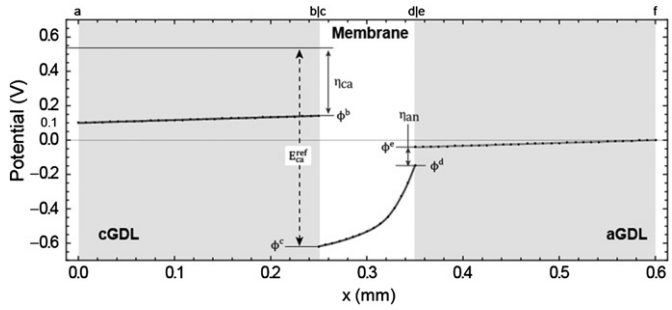

Fig. 4. Potential distribution in MEA under C1 condition.

When the V_{out} is changed along the Cx curve in Fig. 3(a), the potential distributions in the MEA are calculated as in Fig. 5. As the V_{out} goes down, the potential in the cGDL is reduced but its slope is increased as much as the slope in aGDL, because the electric current through the MEA is increased. The change of potential in the membrane is much bigger than the change in the GDL and it has non-linear distribution, which is associated with the water distribution in the membrane. The over-potential in the catalyst layer is also changed with the V_{out} as in Fig. 6. The ratio of η_{ca} to η_{an} is plotted as a dotted curve. It is interesting to note that the ratio changes remarkably with V_{out}. At 1.0 V of V_{out}, η_{ca} is 683 times higher than η_{an}, but their ratio falls to 10 at 0.8 V, and it is 5.17 at 0.6 V. The anode portion in the activation energy increases with the output current density (I_{out}). In many models [7–12,25], η_{an} was easily ignored and their computational domain is restricted to the cathode side. However, Fig. 6 demonstrates that η_{an} has an effect on the cell performance especially at high cell current condition, and both sides should be involved in MEA modeling. The change of potential drop in each layer with the output voltage can be drawn in one figure: over-potential diagram. The diagram, presented in Fig. 7, provides a good understanding on how the electro-chemical energy is used in the MEA. At a high V_{out}, the electro-chemical potential is mainly used for activating the cathode reaction. As the output voltage, $\Delta\phi$(output), decreases, the over-potentials of cCL, aCL, cGDL, membrane, and aGDL, all increase together and the cell can generates more current. In particular, $\Delta\phi$(membrane) increases noticeably due to the low ionic conductivity of the membrane. It means that the conductivity of the membrane becomes the most critical factor for enhancing the cell performance under Cx condition. The over-potential diagram was hardly presented in the literature. The polarization curve was mainly used for validating a model, but this curve is not sufficiently specific for that purpose [30]. If the over-potential diagram is provided, the models of fuel cell are clearly compared and rightly validated.

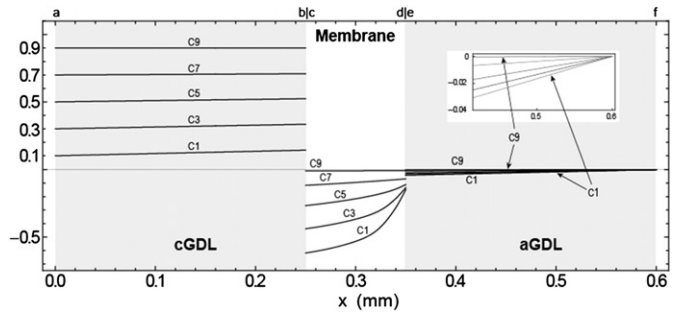

Fig. 5. Potential distributions under Cx conditions.

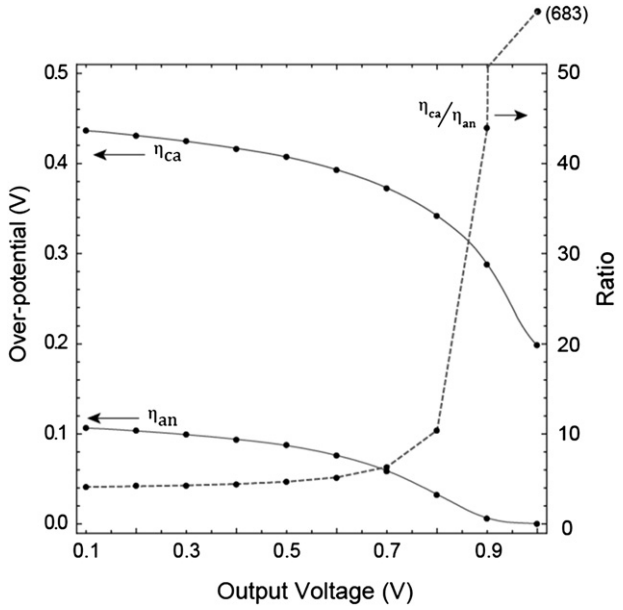

Fig. 6. The over-potentials at cCL and aCL, and their ratio under Cx conditions.

4.2. Current limited by mass diffusion

Fig. 8 shows the potential distributions in the MEA when the supplied O_2 pressure is decreased to 0.2 and 0.05 atm. In this figure, the potential of the membrane and aGDL doesn't change as much as in Fig. 5, when the cell voltage is decreased. This tendency becomes stronger under the lower O_2 pressure condition (Ax), where the potential curves don't seem to change under 0.5 V. It means that the current through the membrane and aGDL is no longer increased, even when the V_{out} is decreased under 0.5 V. The change of over-potentials at catalyst layers are calculated as in Fig. 9. At the conditions of Ax and Bx, the η_{an} becomes fixed, but the η_{ca} is still increased, as the V_{out} is decreased. The increment of η_{ca} doesn't contribute to generating the current flow at the cCL, because O_2 feeding is severely limited as shown in Fig. 10. It is simply wasted as Joule heat [27]. When the supplying pressure of O_2 is decreased in

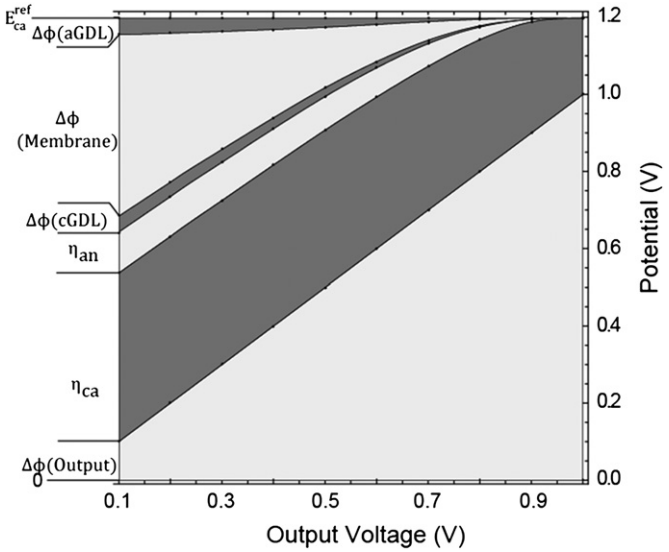

Fig. 7. The over-potential diagram under Cx conditions.

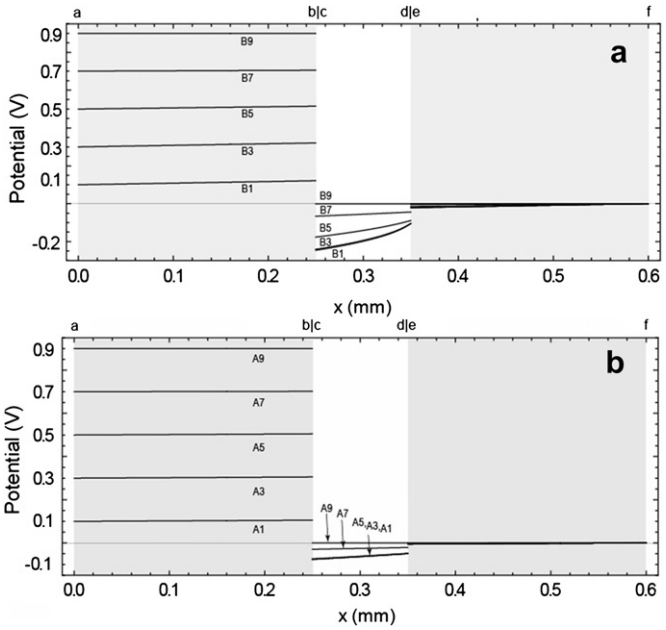

Fig. 8. Potential distributions under (a) Bx and (b) Ax conditions.

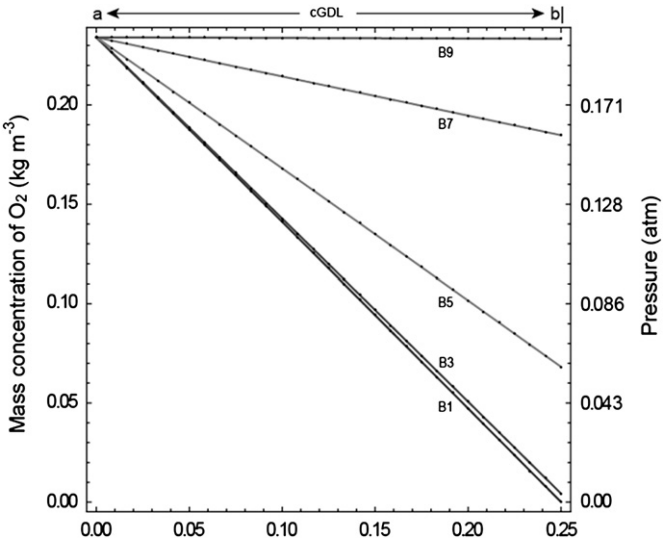

Fig. 10. O_2 concentration distribution in the cGDL under Bx conditions.

the cathode channel, the cell is limited to a lower current value as in Fig. 3 and the η_{an} curve goes down, but the η_{ca} curve goes up as shown in Fig. 9.

The diagram, Fig. 11, shows the over-potential at each layer under the Bx condition. As the cathode reaction becomes restricted by O_2 transfer at a lower cell voltage, only the η_{ca} is expanded and the other over-potentials are fixed. The diagram demonstrates how the electro-chemical energy from fuel cell reaction is consumed at each step and which part is a barrier to better performance. The over-potential of each layer would grow together in a balanced way at a cell of high performance.

4.3. Water transport and ionic conductivity

Fig. 12 shows the vapor water distribution in the GDLs under the Cx condition. Water concentration of positions (a) and (f) are assumed to be saturation value. As decreasing the V_{out} , the vapor concentration increases at position (b|c), but decreases at position (d|e). That is because water is produced from oxygen reduction reaction at cCL. The other reason is Electro-Osmotic Drag (EOD) effect [31] by which water is dragged from the anode to the cathode in membrane. Under Cx conditions, the water content is distributed in the membrane as in Fig. 13. As the current is increased with reducing the V_{out}, water content (λ) goes down at the anode side and goes up at the cathode side. It means that the EOD effect surpasses the back diffusion in membrane, and the effect is enhanced with cell current density. The water concentration is reduced at position (d|e) in Fig. 12, because the membrane absorbs vapor water from the aGDL. The water distribution in membrane is also observed in neutron imaging data [36,37] and other simulation

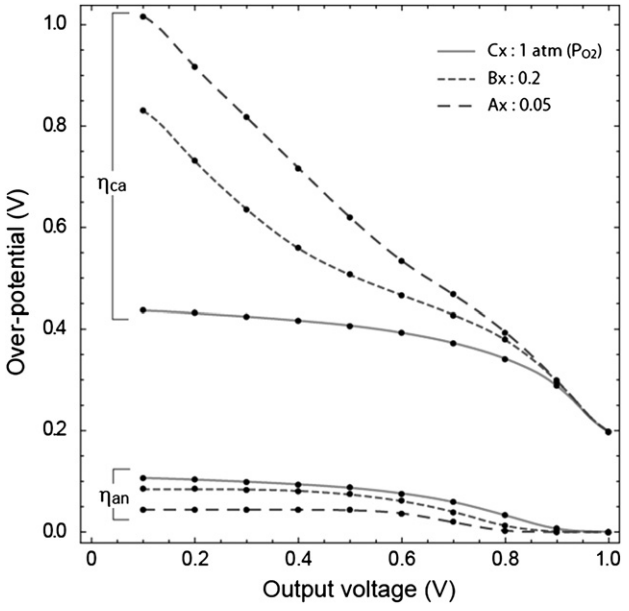

Fig. 9. The over-potentials at cCL and aCL under Ax, Bx, and Cx conditions.

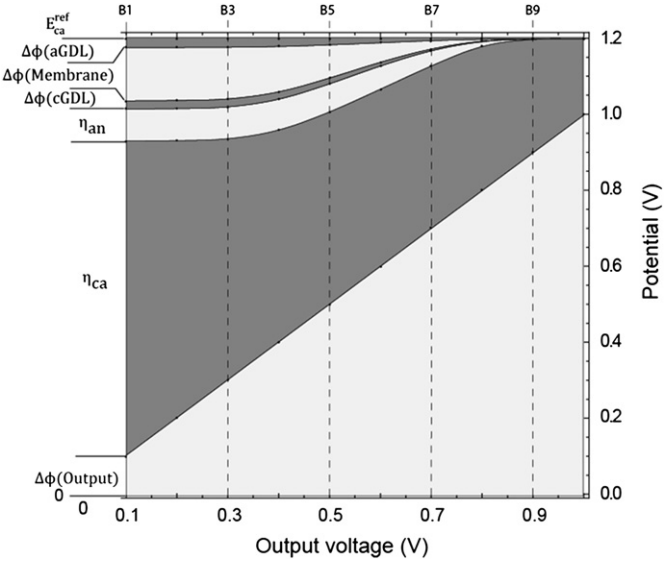

Fig. 11. The over-potential diagram under Bx conditions.

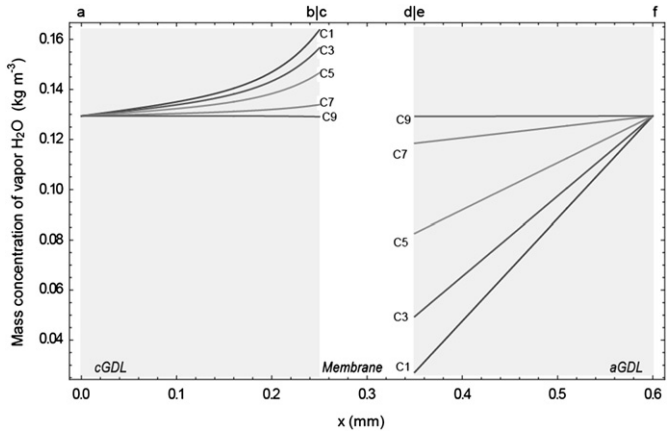

Fig. 12. The distribution of vapor water in GDLs under Cx conditions.

work [38]. The liquid water saturation in the cGDL also increases with decreasing the V_{out}, as in Fig. 14, because of the condensation of over-saturated vapor water.

Water distribution in the membrane has an important effect on the cell performance, because it is related with the ionic conductivity [32]. Fig. 13 also shows the distribution of ionic conductivity. Under C1 condition, the membrane has poor conductivity at the anode side, so that the potential curve has a high gradient at this position in Fig. 4. To compare clearly the overall conductivities of each condition, the effective conductivity ($\overline{\sigma}$) is calculated with the following equations and its values are included in the Fig. 13.

$$\overline{\sigma} = L/\int_0^L \frac{1}{\sigma(x)}\mathrm{d}x \tag{41}$$

As the V_{out} goes down from 0.9 V to 0.1 V, the membrane is dehydrated on the anode side and the water distribution becomes more uneven in the membrane. The ionic conductivity is reduced by 60%. If the reduction rate of the conductivity was not that high,

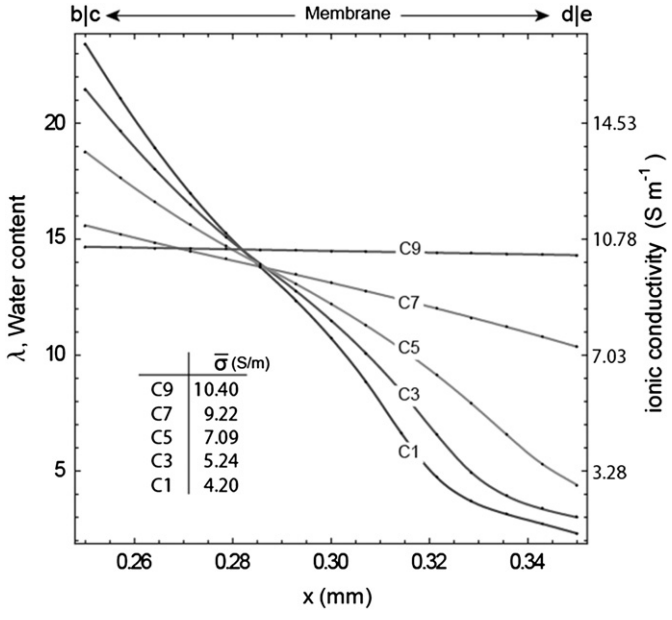

Fig. 13. The distribution of water content and proton conductivity in the membrane under Cx conditions.

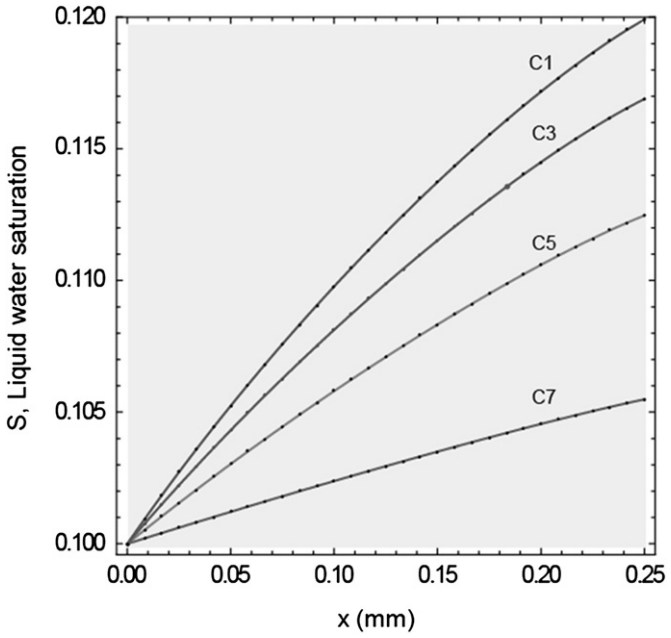

Fig. 14. The distribution of liquid water in the cGDL under Cx conditions.

the membrane would take less over-potential in Fig. 7 and the cell could generate more current.

4.4. Electro-Osmotic Drag(EOD) effect

The EOD in a perfluorosulfonic acid membrane is measured as the EOD coefficient (n_d) which is one of important properties of the membrane. The EOD coefficient is changed with the temperature, membrane hydration level, membrane equivalent weight (EW) and membrane brand [33]. In this work, to analyze quantitatively the

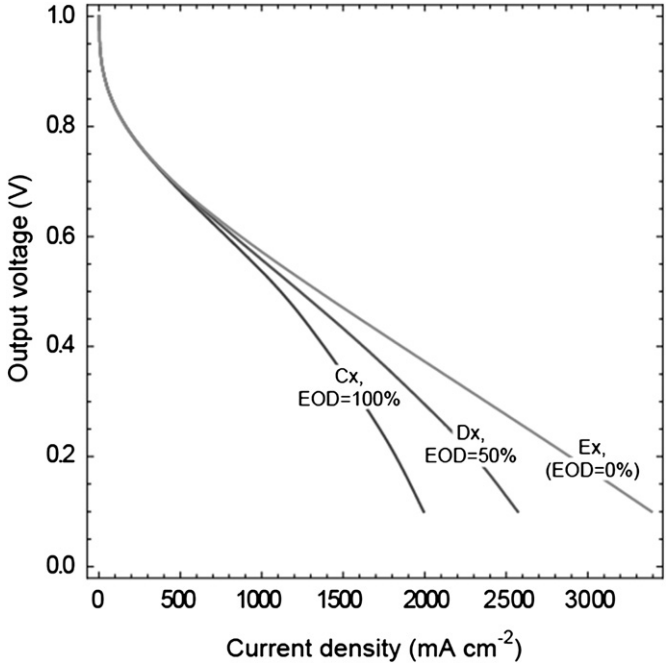

Fig. 15. Polarization curve of the different EODs.

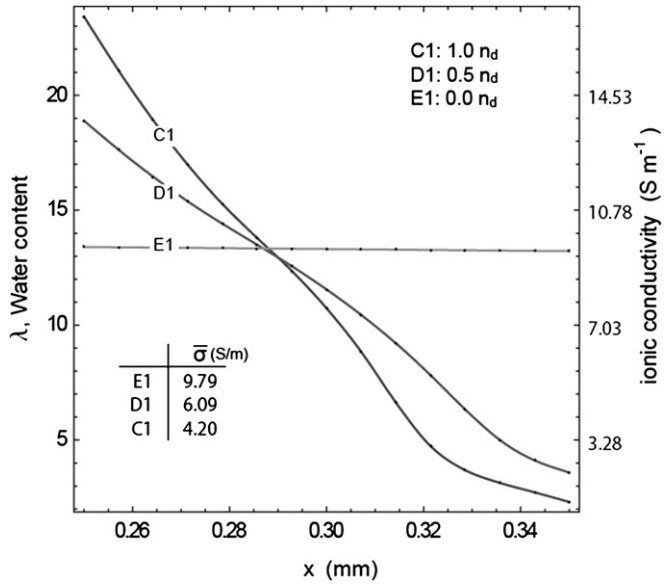

Fig. 16. The distribution of water content and proton conductivity in the membrane under C1, D1 and E1 conditions.

EOD effect on the cell performance, a parametric study is done on the n_d, which is rare in other research papers.

When the n_d, is reduced to 0.5 n_d, and 0.0 n_d under the Cx condition, the polarization curve is changed to Dx and Ex curves in Fig. 15. The difference of the three curves becomes more evident with decreasing the V_{out}, because the EOD effect is enhanced at high current density. The reason that the current density of Ex condition is greater than that of any other condition, is found in the Fig. 16. As the n_d goes down, the water distribution in the membrane becomes even and the effective ionic conductivity is increased. So, the over-potential of the membrane can be reduced and a higher over-potential can be applied to the aCL and cCL, as shown in Fig. 17. The cell current density is increased by 30%(D1) and 70%(E1) from 1993 mA cm^{-2}(C1).

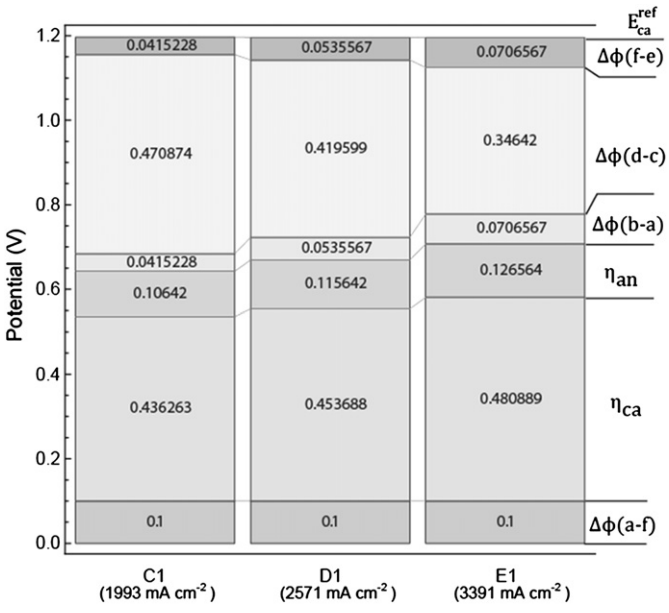

Fig. 17. Over-Potential distributions under C1, D1 and E1 conditions.

5. Conclusions

A two-phase, one-dimensional, and non-isothermal model is successfully developed for simulating the transport phenomena which occurs through the MEA. The model, where the phenomena in the CL are formulated into the boundary conditions for the GDL and the membrane, presents close polarization curves to experimental results.

The change of the potential distribution in the MEA with the cell voltage is plotted in the over-potential diagram. This diagram demonstrates the usage of the electro-chemical energy in the MEA. At a higher output voltages than 0.9 V, most of available energy, over 95%, is taken by the cCL for activating the O_2 reduction reaction as in Fig. 7. As the output voltage is reduced, the over-potential of the membrane is increased more rapidly than of any other layer, which badly affects cell performance at a high current condition. The over-potential ratio of aCL to cCL is not fixed and it is increased at a higher current condition. So, the aCL should be considered as well as the cCL in modeling and designing the MEA of high current density. When the feeding pressure of O_2 to the cathode is decreased, the polarization curve is limited to a lower current. At this condition, only the over-potential of cCL can be increased with decreasing the output voltage, and the electro-chemical energy is wasted as Joule heat at the cCL.

Water distribution in the membrane becomes more uneven, as the output voltage is decreased. That is because the EOD effect intensifies water transport from the anode to the cathode. The uneven distribution of water degrades the ionic conductivity, and the over-potential of membrane is increased. In order that a cell shows better performance, the over-potentials of MEA are balanced, without being concentrated in a layer. The membrane of a smaller EOD coefficient has more even distribution of water, and a smaller over-potential of membrane. Therefore, cell performance is enhanced with reducing this coefficient.

The over-potential diagram provides a good understanding of cell performance with respect to the over-potential of each layer in MEA. The diagram can also be used for validating a fuel cell model.

References

[1] J. Larminie, A. Dicks, Fuel Cell Systems Explained, second ed. John Wiley& Sons, New York, 2003.
[2] R.P. O'Hayre, S.-W. Cha, W. Colella, f.B. Prinz, Fuel Cell Fundamentals, first ed. John Wiley& Sons, New York, 2006.
[3] Y. Wang, K.S. Chen, J. Mishler, S.C. Cho, X.C. Adroher, A review of polymer electrolyte membrane fuel cells: technology, applications, and needs on fundamental research, Appl. Energy 88 (2011) 981–1007.
[4] J. Pander, Hamburg Speeds Up Preparation for Fuel-Cell Cars. Spiegel, SPIE-GELnet GmbH Hamburg, 2009.
[5] J. DeMatio, Kia's big fuel cell plans, in: Automobile Magazine (2009).
[6] Toyota, Toyota advanced fuel cell hybrid vehicle completes Government Field Evaluation, in: PRNewswire (2009).
[7] W.S. He, J.S. Yi, T.V. Nguyen, AlChe J. 46 (10) (2000) 2053–2064.
[8] M. Najjari, F. Khemili, S.B. Nasrallah, Renewable Energy 33 (2008) 1824–1831.
[9] L.X. You, H.T. Liu, Int. J. Hydrogen Energy 26 (2001) 991–999.
[10] J. Liu, N. Oshima, E. Kurihara, L.K. Saha, Transport phenomena within the porous cathode for a proton exchange membrane fuel cell, J. Power Sources 195 (2010) 6342–6348.
[11] N.P. Siegel, M.W. Ellis, D.J. Nelson, M.R. von Spakovsky, Single domain PEMFC model based on agglomerate catalyst geometry, J. Power Sources 115 (2003) 81–89.
[12] R.M. Rao, D. Bhattacharyya, R. Rengaswamy, S.R. Choudhury, A two-dimensional steady state model including the effect of liquid water for a PEM fuel cell cathode, J. Power Sources 173 (2007) 375–393.
[13] G. Lin, W. He, T.V. Nguyen, Modeling liquid water effects in the gas diffusion and catalyst layers of the cathode of a PEM fuel cell, J. Electrochem. Soc. 151 (12) (2004) A1999–A2006.
[14] N.Y. Steiner, Ph. Mocoteguy, D. Candusso, D. hissel, A. Hernadez, A. Aslanides, A review on PEM voltage degradation associated with water management: impacts, influent factors and characterization, J. Power Sources 183 (2008) 260–274.

[15] A.A. Kulikovsky, Quasi-3D modeling of water transport in polymer electrolyte fuel cells, J. Electrochem. Soc. 150 (11) (2003) A1423–A1439.
[16] U. Pasaogullari, C.Y. Wang, Two-phase modeling and flooding prediction of polymer electrolyte fuel cell, J. Electrochem. Soc. 152 (2) (2005) A380–A390.
[17] J.H. Nam, M. Kaviany, Effective diffusivity and water-saturation distribution in single- and two-layer PEMFC diffusion medium, Int. J. Heat Mass Transfer 46 (2003) 4595–4611.
[18] T.E. Springer, T.A. Zawodzinski, S. Gottesfeld, Polymer electrolyte fuel cell model, J. Electrochem. Soc. 138 (8) (1991) 2334–2342.
[19] M. Kaviany, Principles of Heat Transfer in Porous Media, second ed. Springer, New York, 1999.
[20] G.H. Guvelioglu, H.G. Stenger, Computational fluid dynamics modeling of polymer electrolyte membrane fuel cells, J. Power Sources 147 (2005) 95–106.
[21] S. Motupally, A.J. Becker, J.W. Weidner, Diffusion of water in Nafion 115 membranes, J. Electrochem. Soc. 147 (9) (2000) 3171.
[22] T.A. Zawodzinki, T.E. Springer, F. Uribe, S. Gottesfeld, Characterization of polymer electrolytes for fuel cell applications, Solid State Ionics 60 (1993) 199–211.
[23] J. Newman, Electrochemical Systems, second ed. Prentice Hall, New Jersey, 1991.
[24] D. Natarajan, T.V. Nguyen, A two-dimensional, two-phase, multicomponent, transient model for the cathode of a proton exchange membrane fuel cell using conventional gas, J. Electrochem. Soc. 148 (12) (2001) A1324–A1335.
[25] F.P. Incropera, D.P. De Witt, Fundamentals of Heat and Mass Transfer, third ed. John Wiley & Sons, New York, 1990.
[26] A.Z. Weber, J. Newman, Coupled thermal and water management in polymer electrolyte fuel cell, J. Electrochem. Soc. 153 (12) (2006) 2205–2214.
[27] J. Ramousse, O. Lottin, S. Didierjean, D. Maillet, Heat sources in proton exchange membrane (PEM) fuel cells, J. Power Sources 192 (2009) 435–441.
[28] Y.W. Rho, O.A. Velve, S. Srinivasan, Y.T. Kho, Mass transport phenomena in proton exchange membrane fuel cells using O_2/He, O_2/Ar, and O_2/N_2 mixtures, J. Electrochem. Soc. 141 (8) (1994) 2084–2089.
[29] C. He, S. Desai, G. Browns, S. Bollepalli, PEM fuel cell catalysts: cost, performance, and durability, Electrochem. Interface Falls (2005).
[30] C.H. Min, Y.L. He, X.L. Liu, B.H. Yin, w. Jiang, W.Q. Tao, Parameter sensitivity examination and discussion of PEM fuel cell simulation model validation part II, J. Power Sources 160 (2006) 374–385.
[31] T.A. Zawodzinski, C. Derouin, S. Radzinski, R.J. Sherman, V.T. Smith, T.E. Springer, S. Gottesfeld, Water uptake by and transport through Nafion 117 membranes, J. Electrochem. Soc. 140 (1993) 1041–1047.
[32] M.A. Hickner, Cy H. Fujimoto, C.J. Cornelius, Transport in sulfonated polys: proton conductivity, permeability, and the state of water, Polymer 47 (2006) 4238–4244.
[33] X. Ren, S. Gottesfeld, Electro-osmotic drag of water in poly(perfluorosulfonic acid) membranes, J. Electrochem. Soc. 148 (2001) A87–A93.
[34] D.M. Bernardi, Water-balance calculations for solid polymer-electrolyte fuel cell, J. Electrochem. Soc. 137 (8) (1990) 3344–3350.
[35] Y. Wang, C.Y. Wang, A nonisothermal, two-phase model for polymer electrolyte fuel cells, J. Electrochem. Soc. 153 (6) (2006) A1193–A1200.
[36] M.A. Hickner, N.P. Siegel, K.S. Chen, D.S. Hussey, D.L. Jacobson, M. Arif, In situ high-resolution neutron radiography of cross-sectional liquid water profiles in proton exchange membrane fuel cells, J. Electrochem. Soc. 155 (2008) B427–B434.
[37] R. Borup, Water Transport Exploratory Studies (2009) DOE Hydrogen Program Reviews, May 18–22.
[38] Y. Wang, K.S. Chen, Through-plane water distribution in a polymer electrolyte fuel cell: comparison of numerical prediction with neutron radiography data, J. Electrochem. Soc. 157 (2010) B1878–B1886.

Nomenclature

C: Mass concentration of species (kg m^{-3})
D: Diffusion Coefficient (m^2 s^{-1})
s: Liquid water saturation
r: Volumetric condensation rate of water vapor (kg $s^{-1}m^3$)
$\mathbb{C}$: Celsius temperature (°C)
P: Pressure (Pa)
R_g: Universal gas constant (8.314 J $mol^{-1}K^{-1}$)
M: Molecular weight (kg mol^{-1})
$\dot{m}$: Mass flux (kg $s^{-1}m^2$)
K: Absolute permeability (m^2)
K_{rl}: Relative permeability ()
i: Current density (A m^{-2})
ΔH: Condensation heat of water (J kg^{-1})
EW_M: Equivalent molecular weight of the membrane (kg mol^{-1})
F: Faraday Constant (96487 C mol^{-1})
n_d: Drag coefficient of electro-osmosis ()
T: Kelvin Temperature (K)

Superscripts
G: Gas Diffusion layer
M: Membrane

Subscripts
i: Gas species (H_2, O_2)
v: Water vapor
l: Liquid water
c: capillary

Greek
ε: Porosity
γ: Volumetric phase change coefficient (s^{-1})
ρ: Density (kg m^{-3})
μ: Viscosity (N s m^{-2})
σ: Conductivity (S m^{-1})
ϕ: Electrical potential (V)
η: Overpotential (V)
κ: Thermal conductivity (W $m^{-1}K^{-1}$)
ν: Concentration exponent of Oxygen.
λ: Membrane water content.